ChemPubSoc Europe

DOI: 10.1002/chem.201403807

CHEMISTRY
A European Journal
Communication

Solar Cells

Efficient Perovskite Solar Cells with 13.63% Efficiency Based on Planar Triphenylamine Hole Conductors

Hyeju Choi,[a] Sanghyun Paek,[a] Namwoo Lim,[a] Yong Hui Lee,[b] Mohammad Khaja Nazeeruddin,[b] and Jaejung Ko*[a]

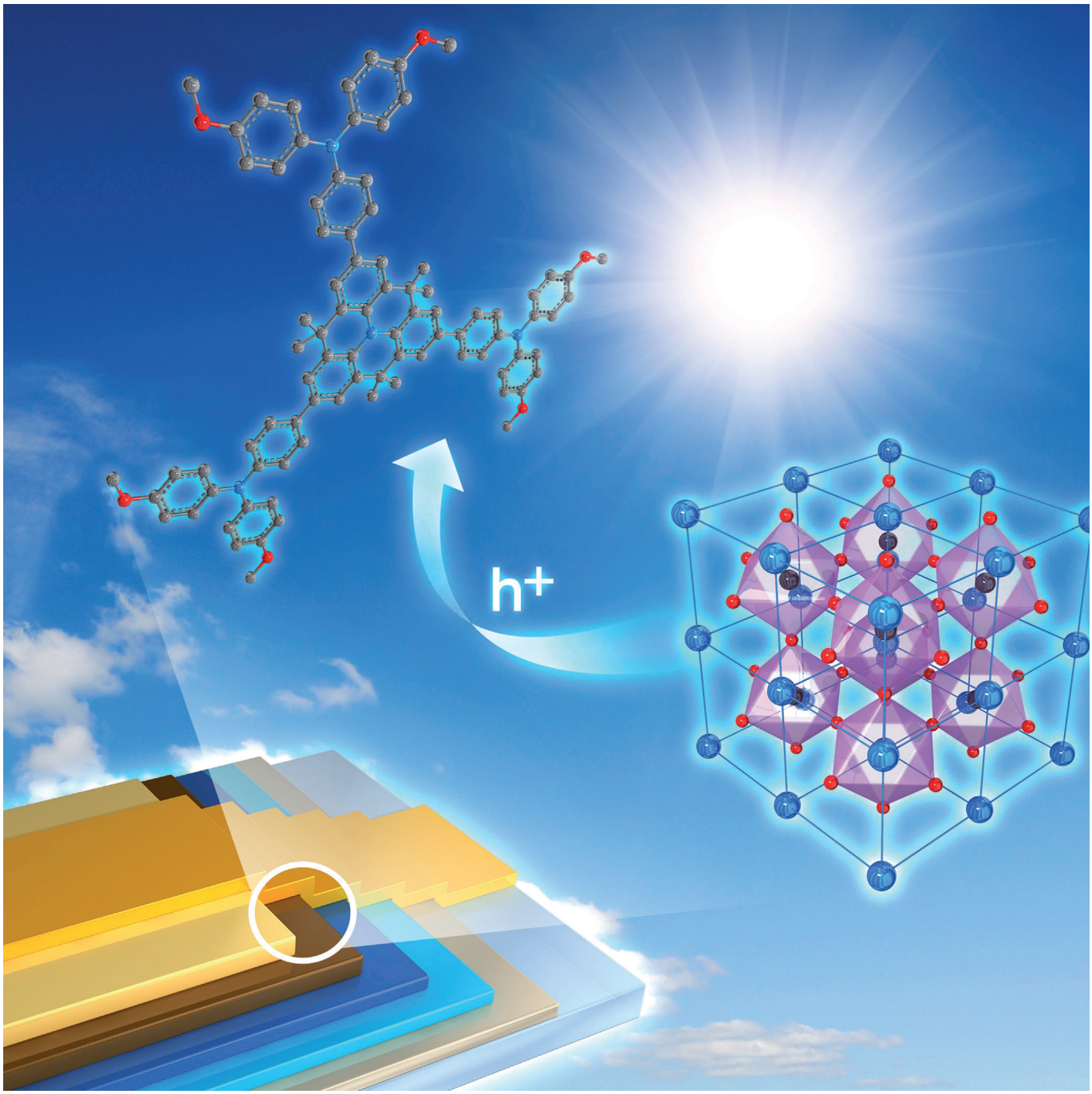

© 2014 Wiley-VCH Verlag GmbH & Co. KGaA, Weinheim

Abstract: A new type of hole transporting material (HTMs) with an incorporated planar amine or triphenylamine as a core unit have been prepared. The two amine derivatives were demonstrated to be efficient hole transporting materials in fabricating solid-state organic–inorganic hybrid solar cells. Perovskite-based solar cells with a planar amine derivative gave a short circuit photocurrent density (J_{sc}) of 20.98 m Acm^{-2}, an open circuit voltage (V_{oc}) of 0.972 V, and a fill factor of 0.67, corresponding to an overall conversion efficiency of 13.63 %. The photovoltaic performance is comparable to that of the standard spiro-OMeTAD. Moreover, the device showed good stability under light soaking for 500 h. These HTMs hold promise to replace the expensive spiro-OMeTAD because of their high efficiency, excellent stability, synthesis from simple and inexpensive materials.

Increasing energy demands and concerns about global warming dictate the development of renewable energy sources.[1] Among several new energy technologies, dye/semiconductor sensitized solar cells (DSSCs) have attracted significant attention as low-cost alternatives to conventional p-n junction solar cells.[2] Although efficient DSSCs have achieved power conversion efficiencies around 11–12 % using a liquid electrolyte such as I^-/I_3^-[3] or Co^{II}/Co^{III} redox couple,[4] stability issues have arisen from its leakage, evaporation of the volatile solvent, and corrosion of the Pt counter electrode by the I^-/I_3^- redox couple. To solve these problems, extensive attempts have been made to substitute liquid electrolytes with solid-state hole conductors[5] or quasi-solid-state electrolytes.[6]

Recently, the organometal halide perovskites have attracted considerable attention as light absorbers for all-solid-state solid cells due to their direct band gap, large absorption coefficient, and high carrier mobility.[7] The hybrid solar cells present a possibility to solve such stability issues by using solid-state p-type hole conductors such as 2,2′,7,7′-tetrakis(*N*,*N*-di-*p*-methoxyphenylamine)-9,9′-spirobifluorene (spiro-OMeTAD),[8] π-conjugated polymers,[9] and $CsSnI_3$ perovskite.[10] An impressive photovoltaic performance was achieved over 15 % power conversion efficiency with spiro-OMeTAD by using a sequential deposition[11] or a dual source thermal evaporation method.[12] In these cells, spiro-OMeTAD appears to be an excellent small hole transporting material (HTM), even though other small molecule HTMs such as 3,4-ethylenedioxythiophene-,[13] pyrene-,[14] and linear π-conjugated structure-based[15] HTMs gave high conversion efficiencies of 12–13 %. However, the sprio-OMeTAD is quite expensive due to its multi-step synthesis and difficulties with purification. For commercial purposes, the exploration of cost-effective HTMs with high efficiency and long stability is urgently required.

Herein, we report new types of hole transporting materials containing a planar amine or star-shape triphenyl amine derivatives, coded as OMeTPA-FA and OMeTPA-TPA, and their application in perovskite-based solar cells. The molecular structure of the two HTMs is shown in Figure 1 a. Our strategy for choosing a fused quinolizino acridine[16] as a core unit is to increase the lifetime of the charge-separated state by the delocalization of the generated cation over a planar amine. The second purpose in choosing such a unit is to mimic the structural framework of *N*,*N*,*N*′,*N*′-tetrakis(4-methoxyphenyl)benzidine (MeO-TPD), which is well recognized as one of the best small molecule HTMs used in ss-DSSCs[17] and OLED[18] as indicated in the three dotted rectangles (Figure 1 a).

The synthetic scheme for the preparation of tris{*N*,*N*-bis(4-methoxyphenyl)-*N*-phenyl}amine quinolizino acridine (OMeTPA-FA) and tris{*N*,*N*-bis(4-methoxyphenyl)-*N*-biphenyl}amine (OMeTPA-TPA) is shown in Figure 1 b. Detailed synthetic procedures are provided in the Supporting Information. The Suzuki coupling reaction[19] of tribromo-quinolizino acridine (**1**) and tris(4-bromophenyl)amine (**2**) with *N*,*N*-bis(4-methoxyphenyl)-*N*-(4-(4,4,5,5,-tetramethyl-1,3,2-dioxaborolan-2-yl)phenyl)amine (**3**) yielded OMeTPA-FA and OMeTPA-TPA in approximately 60 % yield. The analytical and spectroscopic data of both HTMs are consistent with the formulated structures.

The UV/Vis spectra of OMeTPA-FA and OMeTPA-TPA measured in chlorobenzene are shown in the insert of Figure 2 a. The absorption spectrum of OMeTPA-TPA exhibits an intense peak at 374 nm. Under similar conditions, the OMeTPA-FA shows an absorption band at 383 nm that is red-shifted relative to that of OMeTPA. A red-shift of OMeTPA-FA can be readily interpreted by a more planar configuration due to a small torsion angle of the biphenyl unit. The fluorescence spectrum of OMeTPA-FA exhibits a maximum emission at 428 nm, with a small Stokes shift of 55 nm. Two HTMs absorbed light at wavelengths shorter than 420 nm, which overlapped slightly with the absorption band of perovskites. Figure 2 a shows the absorption spectra of the various HTMs processed on the perovskite-coated TiO_2 films, which absorb a broad range of light from visible to the near-infrared. Two HTMs-coated photoactive films exhibit two enhanced absorption bands at 395 and 490 nm due to the superimposed absorption characteristic of their constituents.

Figure 2 b shows the energy level diagram of the respective components in the device. When we deposit a thin layer of OMeTPA-FA or OMeTPA-TPA on the $CH_3NH_3PbI_3$ ($MAPbI_3$) perovskite, the HOMO levels of OMeTPA-FA and OMeTPA-TPA are −5.15 and −5.13 eV, respectively. Therefore, energy levels in the *mp*-TiO_2/$MAPbI_3$/HTM junction are well matched for charge separation and charge transfer at the interface. Figure 2 c shows the device structure of the hybrid solar cells. The cross-

[a] *H. Choi, Dr. S. Paek, N. Lim, Prof. J. Ko*
Department of Advanced Material Chemistry
Korea University, 2511
Sejong-ro, Sejong City 339-700 (Republic of Korea)
Fax: (+82) 41-860-1331
E-mail: jko@korea.ac.kr

[b] *Dr. Y. H. Lee, Dr. M. K. Nazeeruddin*
Laboratory of Photonics and Interfaces
Department of Chemistry and Chemical Engineering
Swiss Federal Institute of Technology
Station 6, 1015 Lausanne (Switzerland)

Supporting information for this article is available on the WWW under http://dx.doi.org/10.1002/chem.201403807.

© 2014 Wiley-VCH Verlag GmbH & Co. KGaA, Weinheim

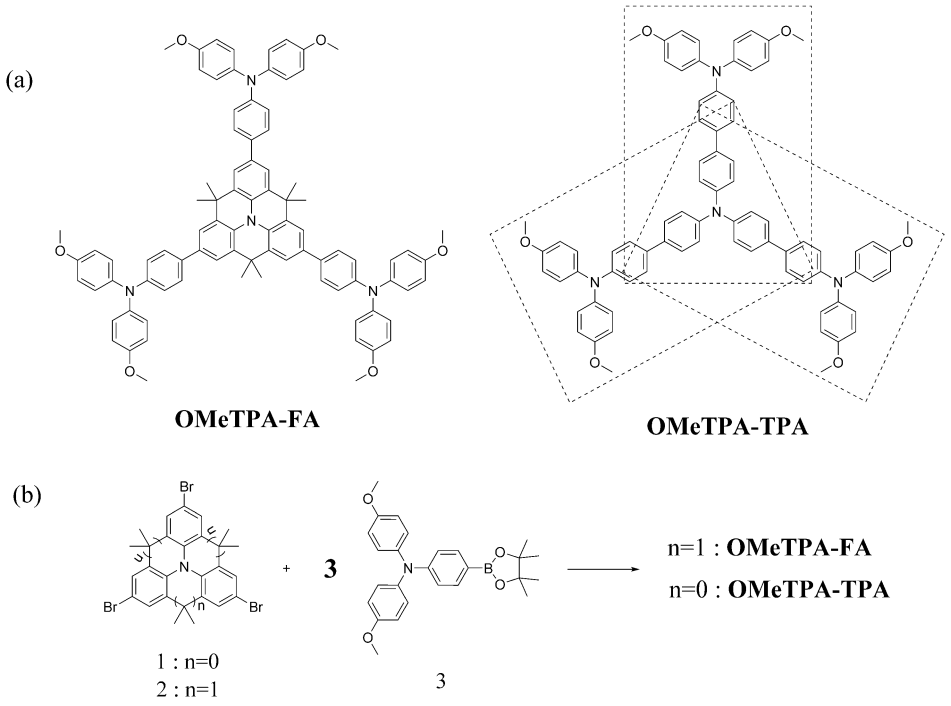

Figure 1. a) Chemical structures of OMeTPA-FA and OMeTPA-TPA. b) Schematic diagram for the synthesis of the OMeTPA-FA and OMeTPA-TPA.

sectional scanning electron microscopy (SEM) images shown in the Figure 2d reveal the formation of a well-defined hybrid structure with sharp interfaces. The thickness of the TiO_2, perovskite, and HTM layer is approximately 300, 200, and 180 nm, respectively, which agrees well with the thicknesses measured using a surface profilometer.

Figure 3a shows photocurrent density–voltage (*J*–*V*) curves for the various devices for the best-performing cells among the 24 devices fabricated using two HTMs. For comparison, the devices without any HTM and with spiro-OMeTAD were fabricated. The device comprising *mp*-TiO_2/$MAPbI_3$/Au without a HTM gives a short circuit photocurrent density (J_{sc}) of 14.28 mAcm^{-2}, an open circuit voltage (V_{oc}) of 0.784 V, and a fill factor (ff) of

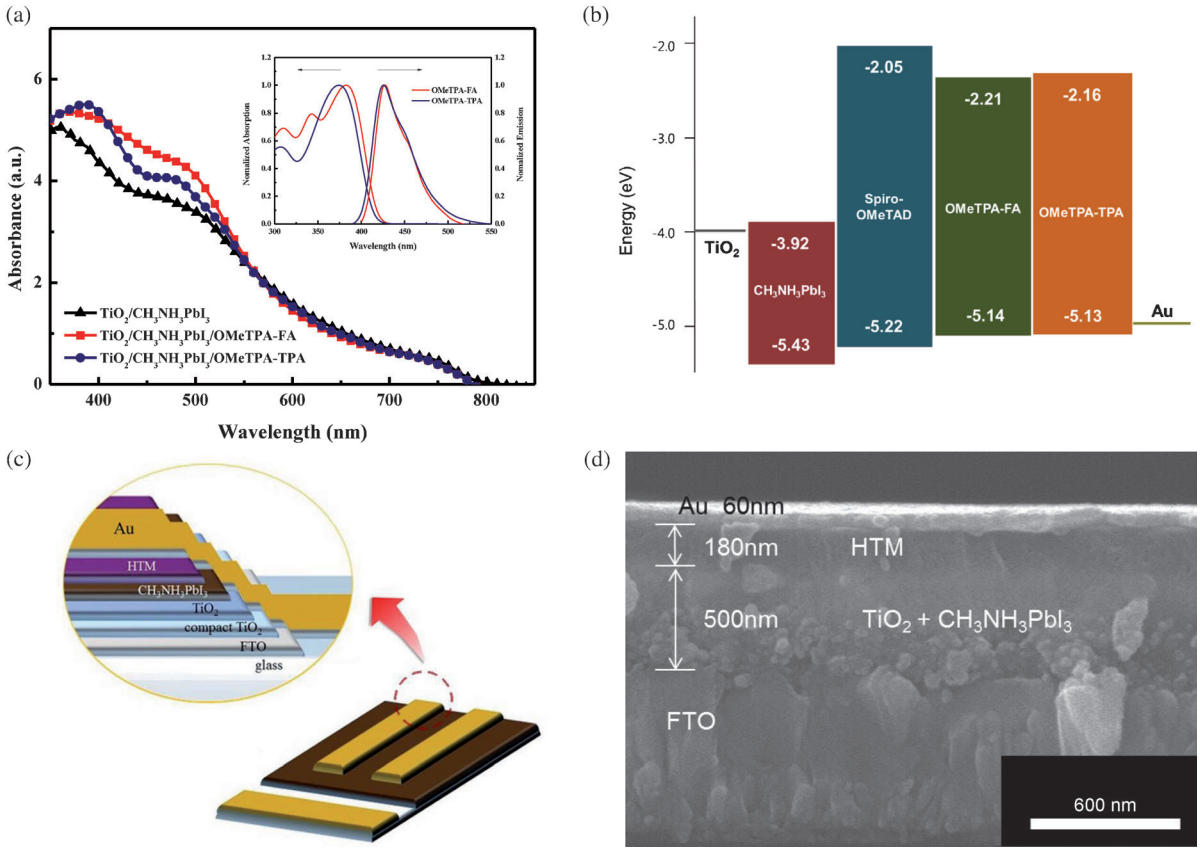

Figure 2. a) UV/Vis absorption spectra of HTMs coated on mp-TiO_2 and mp-TiO_2/$MAPbI_3$ films. Insert: absorption spectra of the HTMs in chlorobenzene. b) Energy level diagram of the HTMs. c) Scheme of the whole device. d) Scanning electron microscopy (SEM) picture of the cross section of the mp-TiO_2/$MAPbI_3$/HTMs/Au.

© 2014 Wiley-VCH Verlag GmbH & Co. KGaA, Weinheim

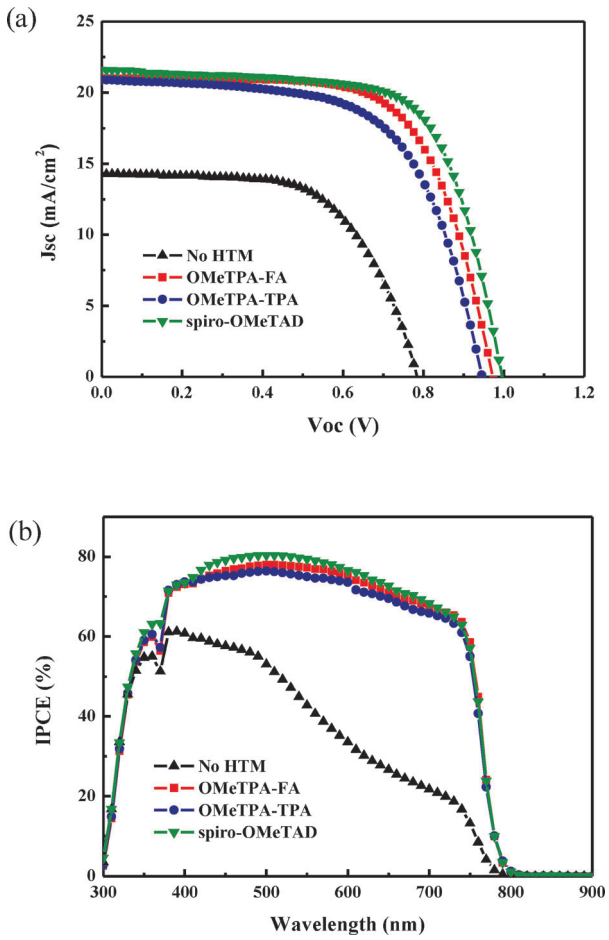

Figure 3. a) Photocurrent–voltage (*J–V*) curves and b) IPCE spectrum of the devices.

0.61, affording an overall conversion efficiency of 6.85%. These values are comparable to those reported by Etgar et al.[20] On the other hand, the devices in the presence of HTMs exhibit remarkably improved photovoltaic performances. The device comprising *mp*-TiO_2/$MAPbI_3$/OMeTPA-FA/Au without any additives in HTM gave a J_{sc} of 19.42 m Acm^{-2}, a V_{oc} of 0.905 V, and a ff of 0.63, corresponding to an overall conversion efficiency of 11.7%. As the solid-state sensitized solar cells have exhibited an impressive enhancement in PCE by increasing the conductivity of HTMs via doping the additives such as 4-*tert*-butylpyridine (*t*-Bp) and lithium bis(trifluoromethane-sulfonyl)imide (Li-TFSI) into the spiro-OMeTAD,[21] we attempted to fabricate the devices by doping the two additives into the OMeTPA-FA or OMeTPA-TPA hole conductor. The *mp*-TiO_2/$MAPbI_3$/OMeTPA-FA/Au device prepared with two additives exhibited a J_{sc} of 20.53 m Acm^{-2}, a V_{oc} of 0.925 V, and a ff of 0.65, corresponding to a PCE of 12.40%. A substantial increase in PCE form 11.07 to 12.40% by adding two dopants into the HTM may be interpreted as the increase of hole conductivity in HTM. However, the photovoltaic parameter that still diminishes the efficiency in these perovskite-based solar cells is the fill factor, which is lower than those found for other perovskite hybrid cells. Recently, Burschka et al[22] reported that the addition of a p-type cobalt(III) complex with two additives (*t*-Bp and Li-TFSI) to spiro-OMeTAD enhanced the photovoltaic performances, in particular, fill factor, by ensuring a high conductivity. The device prepared with the three dopants into the OMeTPA-FA gave an average efficiency of 12.67% and the highest efficiency of 13.63%. The best-performing device gave a J_{sc} of 20.98 mAcm^{-2}, a V_{oc} of 0.972 V, and a ff of 0.67, affording a PCE of 13.63%. Under the same conditions, the OMeTPA-TPA and spiro-OMeTAD based cells gave a J_{sc} of 20.88 and 21.57 m Acm^{-2}, a V_{oc} of 0.946 and 0.996 V, and a ff of 0.62 and 0.68, corresponding to η of 12.31 and 14.68%, respectively. The photocurrent action spectra of the three devices using three dopants into the HTMs are presented in the Figure 3 b. The incident-photon-to-current conversion efficiency (IPCE) of the *mp*-TiO_2/$MAPbI_3$/OMeTPA-FA/Au device exceeds 75% in a broad spectral range from 380 to 740 nm, reaching its maximum of 80% at approximately 500 nm. The integrated photocurrent density is 20.22 m Acm^{-2}, which is in good agreement with the measured photocurrent density of 20.98 m Acm^{-2} at the standard solar AM 1.5 G. The J_{sc} value measured with above three devices are quite similar. On the other hand, the V_{oc} and ff of three deices differed significantly. From the above results, we have observed that the η value of a spiro-OMeTAD based solar cell is higher than that of OMeTPA-FA or OMeTPA-TPA based cells due to a high V_{oc} and fill factor. The V_{oc} trend for three devices fabricated by using OMeTPA-FA, OMeTPA-TPA, and spiro-OMeTAD as HTMs is in agreement with the relative difference in the HOMO levels of three HTMs because the energy level offset between the HOMO level of the donor and the LUMO level of the acceptor modulates the magnitude of V_{oc}.

Table 1 shows that the lower performance of the *mp*-TiO_2/$MAPbI_3$/OMeTPA-TPA/Au device compared with that of devices with OMeTPA-FA or spiro-OMeTAD as HTM may be attributable to the poor fill factor. The fill factor is known to be closely related to both series resistance (R_s) of solar cell and hole mobility of HTMs. To obtain a high fill factor, the solar cells should have a low series resistance and high conductivity. From the slope of the *J–V* curve around the V_{oc}, the R_s value of OMeTPA-FA, OMeTPA-TPA, and spiro-OMeTAD are calculated to be 12.8, 16.8, and 10.5 Ω cm^{-2}, respectively. The PCE enhancement of

Table 1. Summary of photovoltaic parameters derived from *J–V* measurements of $CH_3NH_3PbI_3$ based devices.[a]

HTM	J_{sc} [mAcm^{-2}]	V_{oc} [V]	ff	η [%]
no HTM	14.28	0.784	0.61	6.85
OMeTPA-FA[b]	19.42	0.905	0.63	11.07
OMeTPA-FA[c]	20.53	0.925	0.65	12.40
OMeTPA-FA[d]	20.98	0.972	0.67	13.63
OMeTPA-TPA[c]	19.49	0.934	0.60	10.97
OMeTPA-TPA[d]	20.88	0.946	0.62	12.31
spiro-OMeTAD[d]	21.57	0.996	0.68	14.68

[a] The photovoltaic characteristics are performed under simulated 100 m Wcm^{-2} AM 1.5G illumination. The masked active area of device is 0.16 cm^2. [b] Without any additives. [c] Addition of *t*-Bp and LiTFSI. [d] Addition of *t*-Bp, Li-TFSI, and cobalt dopant(FK209).

© 2014 Wiley-VCH Verlag GmbH & Co. KGaA, Weinheim

the *mp*-TiO_2/$MAPbI_3$/spiro-OMeTAD/Au device relative to the *mp*-TiO_2/$MAPbI_3$/OMeTPA-FA/Au or *mp*-TiO_2/$MAPbI_3$/OMeTPA-TPA/Au ones can be related to the lower value of R_s. To clarify the effect of hole mobility on the photovoltaic performance, we measured the hole mobility of HTMs from the space charge limitation of current (SCLC) *J–V* characteristics obtained in the dark. The hole mobilities of OMeTPA-FA, OMeTPA-TPA, and spiro-OMeTAD evaluated by using the Mott–Gurney law[23] were calculated to be 3.67×10^{-4}, 1.08×10^{-4}, and 4.53×10^{-4}, $cm^2V^{-1}S^{-1}$, respectively. The high hole mobility of the *mp*-TiO_2/$MAPbI_3$/spiro-OMeTAD/Au device compared with other two devices led to an improved fill factor. Therefore, the fill factor of the devices followed a trend that is proportional to the value of high mobility and low series resistance.

Figure 4 shows the photovoltaic performances during long-term aging test of three devices using three dopants composed of *t*-Bp, LiTFSI, and Co^{III} complex into the HTMs. The PCE

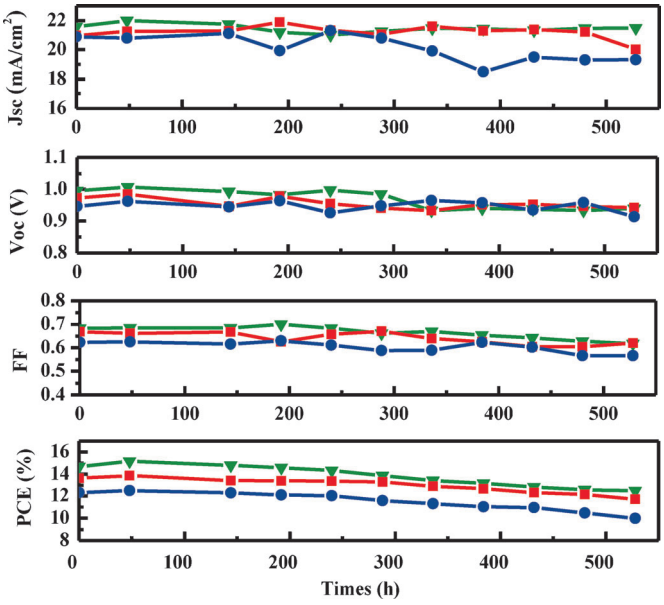

Figure 4. Evolution of solar-cell parameters with OMeTPA-FA(●), OMeTPA-TPA(■), and spiro-OMeTAD(▼)-based cell stored in air at room temperature under one sun illumination.

for the OMeTPA-FA and spiro-OMeTAD based cells in air without any encapsulation gradually decreased as the aging time increased. After 500 h of aging, the initial efficiency of 13.24% in the OMeTPA-FA based device decreased to 11.64%, giving a 12% reduction. This reduction is almost similar to that of the spiro-OMeTAD based cell (10.82%). On the other hand, the initial efficiency of 12.28% in the OMeTPA-TPA based cell sharply decreased to 9.54%, giving a 22.31% reduction. The relative stability for the OMeTPA-FA based cell relative to the OMeTPA-TPA one may be attributable to the well packing on the $MAPbI_3$ layer due to a planar molecule configuration.

In summary, we designed and synthesized two efficient hole conductors containing a fused triphenylamine and triphenylamine moiety. The solid-state perovskite based device using OMeTPA-FA as a HTM yielded an overall conversion efficiency of 13.63%, which is comparable to that (14.68%) of the spiro-OMeTAD based cell. Moreover, the OMeTPA-FA based device stored for 500 h with any encapsulation under outdoor conditions retained its photovoltaic performances. We believe that the development of highly efficient hybrid solar cells with robustness is possible through the structural modification of hole conductors by tuning the HOMO level, and work on these is now in progress.

Experimental Section

Synthesis and characterization of materials: All reactions were carried out under an argon atmosphere. Solvents were distilled from appropriate reagents. All reagents were purchased from Sigma–Aldrich and TCI. Bis(*N*,*N*-(4-methoxyphenyl)-*N*-(4-(4,4,5,5-tetramethyl-1,3,2-dioxaborolan-2-yl)phenyl))amine[24] and tri-bromotriarylamine[25] were prepared according to the literature procedure.

Tis{*N*,*N*-bis((4-methoxyphenyl)amino)biphenyl}-amine (OMeTPA-TPA): A mixture of boron compound (2.78 mmol, 1.2 g), tris(4-bromophenyl)amine (0.62 mmol, 0.3 g), 2 M solution of K_2CO_3 (9.33 mmol, 1.29 g) in H_2O (4.65 mL), [$Pd(PPh_3)_4$] (0.062 mmol, 0.072 g) in dry THF (50 mL) was refluxed for 48 h. After cooling the solution, the organic layer was removed in vacuo. The crude product was extracted with CH_2Cl_2 and dried in $MgSO_4$. The pure product OMeTPA-TPA was obtained by silica gel chromatography using a mixture of ethyl acetate and *n*-hexane (1:5) as an eluent (yield 65%). ^1H NMR (300 MHz, $CDCl_3$, 25 °C): $\delta=7.45$ (d, $J=8.4$ Hz, 6H), 7.40 (d, $J=9.3$ Hz, 6H), 7.18 (d, $J=8.4$ Hz, 6H), 7.09 (d, $J=9.3$ Hz, 12H), 6.99 (d, $J=9.3$ Hz, 12H), 6.84 (d, $J=8.3$ Hz, 6H), 3.81 ppm (s, 18H); ^{13}C NMR (75 MHz, $CDCl_3$, 25 °C): $\delta=155.9$, 147.8, 146.4, 141.1, 135.3, 132.8, 128.0, 127.1, 127.0, 126.6, 121.1, 115.7, 114.8, 55.6 ppm; MS: *m/z* 1155 [M^+]; elemental analysis calcd (%) for $C_{78}H_{66}N_4O_6$: C 81.08, H 5.76; found : C 80.62; H 5.52.

Tis{*N*,*N*-bis((4′-methoxyphenyl)amino)phenyl}-fused amine (OMeTPA-FA): A mixture of boron compound (2.24 mmol, 0.97 g), tribromo fused amine (0.50 mmol, 0.3 g), 2 M solution of K_2CO_3 (7.47 mmol, 1.03 g) in H_2O (3.74 mL), [$Pd(PPh_3)_4$] (0.050 mmol, 0.058 g) in dry THF (50 mL) was refluxed for 48 h. After cooling the solution, the organic layer was removed in vacuo. The crude product was extracted with CH_2Cl_2 and dried in $MgSO_4$. The pure product OMeTPA-FA was obtained by silica gel chromatography using a mixture of ethyl acetate and *n*-hexane (1:7) as an eluent (yield 62%). ^1H NMR (300 MHz, $CDCl_3$, 25 °C): $\delta=7.57$ (s, 6H), 7.47 (d, $J=6.9$ Hz, 6H), 7.11 (d, $J=8.7$ Hz, 12H), 7.04 (d, $J=7.8$ Hz, 6H), 7.86 (d, $J=6.9$ Hz, 12H), 3.81 ppm (s, 18H), 1.74 (s, 18H); ^{13}C NMR (75 MHz, $CDCl_3$, 25 °C): $\delta=155.8$, 147.8, 141.3, 128.8, 128.3, 127.8, 122.2, 121.5, 120.5, 115.5, 114.8, 114.0, 55.7, 31.5, 25.1 ppm; MS: *m/z* 1275 [M^+]; elemental analysis calcd (%) for $C_{87}H_{78}N_4O_6$: C, 81.92, H 6.16; found : C 81.44, H 6.04.

Measurements and instruments: ^1H and ^{13}C NMR spectra were recorded on a Varian Mercury 300 spectrometer. Elemental analyses were performed with a Carlo Elba Instruments CHNS-O EA 1108 analyzer. Mass spectra were recorded on a JEOL JMS-SX102A instrument. The absorption and photoluminescence spectra were recorded on a PerkinElmer Lambda 2S UV-visible spectrometer and a Perkin LS fluorescence spectrometer, respectively. Cyclic voltammetry was carried out with a BAS 100B (Bioanalytical System, Inc.). A three-electrode system was used and consisted of non-aqueous reference electrode (0.1 M Ag/Ag^+ acetonitrile solution; MF-2062, Bioanalytical System, Inc.), platinum working electrode (MF-2013,

© 2014 Wiley-VCH Verlag GmbH & Co. KGaA, Weinheim

Bioanalytical System, Inc.), and a platinum wire (diam. 1.0 mm, 99.9% trace metals basis, Sigma–Aldrich) as counter electrode. Redox potential of dyes was measured in $CHCl_3$ with 0.1 M (n-$C_4H_9)_4N$-PF_6 with a scan rate between 100 mVs^{-1} (vs. external Fc/Fc^+). Solar cells efficiencies were characterized under simulated 100 $mWcm^{-2}$ AM 1.5G irradiation from a Xe arc lamp with an AM 1.5 global filter. Simulator irradiance was characterized using a calibrated spectrometer and illumination intensity was set using an NREL certified silicon diode with an integrated KG1 optical filter: spectral mismatch factors were calculated for each device in this report to be less than 5%. Short circuit currents were also found to be with 5% of values calculated using the integrated external quantum efficiency (EQE) spectra and the solar spectrum. The EQE was measured by underfilling the device area using a reflective microscope objective to focus the light output from a 75 watt Xe lamp, monochromator, and optical chopper; photocurrent was measured using a lock-in amplifier and the absolute photon flux was determined by a calibrated silicon photodiode.

Device fabrication: FTO glass plates (Pilkington, TEC-8) were cleaned in a detergent solution using an ultrasonic bath for 30 min, rinsed with water and ethanol. The compact TiO_2 layer was deposited on the etched F-doped tin oxide substrate by spray pyrolysis at 450 °C, using titanium diisopropoxide bis(acetylacetonate) solution. The FTO glass plates were immersed in 40 mM $TiCl_4$ (aqueous) at 70 °C for 30 min and and sintered at 500 °C for 30 min. Mesoporous TiO_2 films was deposited by spin coating of a diluted TiO_2 paste (Dyesol 18NR-T, 1:3.5w/w diluted with ethanol) at 5000 rpm for 30 s. The films were sintered at 500 °C. The PbI_2 in DMF solution (1.0 M) was dropped on the TiO_2/FTO substrate by spin-coating at 6500 rpm for 30 s, and dried on a hot plate at 70 °C for 30 min. After cooling down, the film was dipped into a CH_3NH_3I/2-propanol solution (8 mg mL^{-1}) for 25 s, and dried at 70 °C for 15 min. The HTMs (0.052 M in chlorobenzene) were spin-cast on top of the $CH_3NH_3PbI_3/TiO_2$/FTO substrate at 3000 rpm. Finally, the device was pumped down to lower than 10^{-5} torr and a ~60 nm thick Au counter electrode was deposited on top.

Acknowledgements

This work was supported by the International Science and Business Belt Program through the Ministry of Science, ICT and Future Planning (No. 2012K001573), ERC (the Korean government (MEST)) program (No. 20120000591), and Basic Science Research Program through the National Research Foundation of Korea (NRF) funded by the Ministry of Education (2013R1A1A4A01005961).

Keywords: hole transporting material · perovskites · solar cells

[1] N. Robertson, *Angew. Chem.* **2006**, *118*, 2398 – 2405; *Angew. Chem. Int. Ed.* **2006**, *45*, 2338 – 2345.

[2] a) B. O'Regan, M. Grätzel, *Nature* **1991**, *363*, 737 – 740; b) M. Grätzel, *Nature* **2001**, *414*, 338 – 344.

[3] a) J.-H. Yum, E. Baranoff, F. Kessler, T. Moehl, S. Ahmad, T. Bessho, A. Marchioro, E. Ghadiri, J.-E. Moser, C. Yi, M. K. Nazeeruddin, M. Grätzel, *Nat. Commun.* **2012**, *3*, 631; b) M. K. Kashif, J. C. Axelson, N. W. Duffy, C. M. Forsyth, C. J. Chang, J. R. Long, L. Spiccia, U. Bach, *J. Am. Chem. Soc.* **2012**, *134*, 16646 – 16653.

[4] A. Yella, H.-W. Lee, H. N. Tsao, C. Yi, A. K. Chandiran, M. K. Nazeeruddin, E. W. G. Diau, C.-Y. Yeh, S. M. Zakeeruddin, M. Grätzel, *Science* **2011**, *334*, 629 – 634.

[5] a) M. Wang, M. Xu, D. Shi, R. Li, F. Gao, G. Zhang, Z. Yi, R. Humphry-Baker, P. Wang, S. M. Zakeeruddin, M. Grätzel, *Adv. Mater.* **2008**, *20*, 4460 – 4463; b) N. Cai, S.-J. Moon, L. Cevey-Ha, T. Moehl, R. Humphry-Baker, P. Wang, S. M. Zakeeruddin, M. Grätzel, *Nano Lett.* **2011**, *11*, 1452 – 1456.

[6] a) C.-L. Chen, H. Teng, Y.-L. Lee, *Adv. Mater.* **2011**, *23*, 4199 – 4204; b) H. Choi, S. O. Kang, J. Ko, G. Gao, H. S. Kang, M.-S. Kang, M. K. Nazeeruddin, M. Grätzel, *Angew. Chem.* **2009**, *121*, 6052 – 6055; *Angew. Chem. Int. Ed.* **2009**, *48*, 5938 – 5941.

[7] a) H.-S. Kim, C.-R. Lee, J.-H. Im, K.-B. Lee, T. Moehl, A. Marchioro, S.-J. Moon, R. Humphry-Baker, J.-H. Yum, J. E. Moser, M. Grätzel, N.-G. Park, *Sci. Rep.* **2012**, *2*, 591; b) M. M. Lee, J. Teuscher, T. Miyasaka, T. N. Murakami, H. J. Snaith, *Science* **2012**, *338*, 643 – 647.

[8] a) H.-S. Kim, S. H. Im, N.-G. Park, *J. Phys. Chem. C* **2014**, *118*, 5615 – 5625; b) J.-H. Yum, C.-R. Lee, J.-W. Lee, S.-W. Park, N.-G. Park, *Nanoscale* **2011**, *3*, 4088 – 4093; c) D. Liu, T. L. Kelly, *Nature Photonics* **2014**, *8*, 133 – 138; d) G. E. Eperon, S. D. Stranks, C. Menelaou, M. B. Johnston, L. M. Herz, H. J. Snaith, *Energy Environ. Sci.* **2014**, *7*, 982 – 988.

[9] a) J. H. Heo, S. H. Im, J. H. Noh, T. N. Mandal, C.-S. Lim, J. A. Chang, Y. H. Lee, H.-J. Kim, A. Sarkar, M. K. Nazeeruddin, M. Grätzel, S. I. Seok, *Nature Photonics* **2013**, *7*, 486 – 491; b) B. Cai, Y. Xing, Z. Yang, W.-H. Zhang, J. Qiu, *Energy Environ. Sci.* **2013**, *6*, 1480 – 1485; c) Y. S. Kwon, J. Lim, H.-J. Yum, Y.-H. Kim, T. Park, *Energy Environ. Sci.* **2014**, *7*, 1454 – 1460; d) B. Conings, L. Baeten, C. D. Dobbelaere, J. D'Haen, J. Manca, H.-G. Boyen, *Adv. Mater.* **2014**, *26*, 2041 – 2046.

[10] I. Chung, B. Lee, J. He, R. P. H. Chang, M. G. Kanatzidis, *Nature* **2012**, *485*, 486 – 489.

[11] J. Burschka, N. Pellet, S.-J. Moon, R. Humphry-Baker, P. Cao, M. K. Nazeeruddin, M. Grätzel, *Nature* **2013**, *499*, 316 – 319.

[12] M. Liu, M. B. Johnston, H. J. Snaith, *Nature* **2013**, *501*, 395 – 398.

[13] H. Li, K. Fu, A. Hagfeldt, M. Grätzel, S. G. Mhaisalkar, A. C. Grimsdale, *Angew. Chem. Int. Ed.* **2014**, *53*, 4085 – 4088; *Angew. Chem.* **2014**, *126*, 4169 – 4172.

[14] N. J. Jeon, J. Lee, J. H. Noh, M. K. Nazeeruddin, M. Grätzel, S. I. Seok, *J. Am. Chem. Soc.* **2013**, *135*, 19087 – 19090.

[15] J. Wang, S. Wang, X. Li, L. Zhu, Q. Meng, Y. Xiao, D. Li, *Chem. Commun.* **2014**, *50*, 5829 – 5832.

[16] a) D. Hellwinkel, M. Melan, *Chem. Ber.* **1974**, *107*, 616 – 626; b) S. Bamberger, D. Hellwinkel, F. A. Neugebauer, *Chem. Ber.* **1975**, *108*, 2416 – 2421.

[17] L. Yang, B. Xu, D. Bi, H. Tian, G. Boschloo, L. Sun, A. Hagfeldt, E. M. J. Johansson, *J. Am. Chem. Soc.* **2013**, *135*, 7378 – 7385.

[18] K. Walzer, B. Maenning, M. Pfeiffer, K. Leo, *Chem. Rev.* **2007**, *107*, 1233 – 1271.

[19] a) C.-H. Huang, N. D. McClenaghan, A. Kuhn, J. W. Hofstraat, D. M. Bassan, *Org. Lett.* **2005**, *7*, 3409 – 3412; b) K. J. Hoffmann, E. Bakken, E. J. Samuelsen, P. H. J. Carlen, *Synth. Met.* **2000**, *113*, 39 – 44.

[20] L. Etgar, P. Cao, Z. Xue, Q. Peng, A. K. Chandiran, B. Liu, M. K. Nazeeruddin, M. Grätzel, *J. Am. Chem. Soc.* **2012**, *134*, 17396 – 17399.

[21] H. J. Snaith, M. Grätzel, *Appl. Phys. Lett.* **2006**, *89*, 262114.

[22] J. Burschka, A. Dualeh, F. Kessler, E. Baranoff, N.-L. Cevey-Ha, C. Yi, M. K. Nazeeruddin, M. Grätzel, *J. Am. Chem. Soc.* **2011**, *133*, 18042 – 18045.

[23] V. D. Mihailetchi, H. Xie, B. de Boer, L. J. A. Koster, P. W. M. Blom, *Adv. Funct. Mater.* **2006**, *16*, 699 – 708.

[24] L. Yu, J. Xi, H. T. Chan, T. Su, L. J. Antrobus, B. Tong, Y. Dong, W. K. Chan, D. L. Phillips, *J. Phys. Chem. C* **2013**, *117*, 2041 – 2052.

[25] Z. Fang, V. Chellappan, R. D. Webster, L. Ke, T. Zhang, B. Liud, Y.-H. Lai, *J. Mater. Chem.* **2012**, *22*, 15397 – 15404.

Received: June 9, 2014
Published online on August 5, 2014

Please note: Minor changes have been made to this manuscript since its publication in *Chemistry—A European Journal* Early View. The Editor.

© 2014 Wiley-VCH Verlag GmbH & Co. KGaA, Weinheim